PENETRATION MECHANICS OF EXTENDING HEMICYLINDRICAL RODS

David L. Littlefield, Ph.D and William G. Reinecke, Ph.D.

Institute for Advanced Technology, 3925 W. Braker Ln., Austin, TX 78759, USA

The purpose of this numerical study is to examine the effect of cross section geometry on the penetration mechanics of extending hemicylindrical rods. The impact velocity is 2.2 km/s. Here, the cross section is varied by changing the relative dimensions of the tongue/slot geometry for the fore and aft sections of the rod. It is shown that the slot geometry can have a significant impact on the performance of the penetrator. Narrow slots tend to produce cavities that exhibit sidewall interference, whereas deeply protruding slots result in cavities with exaggerated lateral dimensions. As such, the optimum slot geometry occurs for an intermediate condition. At this optimum, numerical results predict that no degradation in penetration occurs when compared to constant mass, constant length cylindrical rods.

INTRODUCTION

Extending rods show great promise as a means of increasing the effective length and performance of long rod penetrators. This is particularly true at velocities above 2 km/s, where penetration efficiency is less sensitive to the aspect ratio of the rod. A variety of cross-section geometries have been proposed that are amenable to extension; examples of these include the so-called "tuning fork" and "rod-tube" configurations. At first glance these geometries appear to be attractive candidates for achieving extension, since mass centers of the leading and trailing cross sections are coincident. However, a common feature to all these geometries is a "leg" or "tube" portion of the extending rod, which can exhibit reduced penetration efficiency when compared to the rest of the rod.

The penetration mechanics of alternative geometries for extension are investigated in this numerical study. Here, the cross-section geometries of the extended portions do not have the same mass centers. The simplest rendition of this geometry is two offset hemicylinders. This configuration was first suggested by Barnette [1] as a possible configuration for an extending rod and is investigated in detail here. Calculations have been performed using the Eulerian hydrocode CTH, which suggest the enhanced performance of this configuration. It is shown that the crater geometries formed from this penetrator avoid many of the difficulties encountered with the "in-line" geometries.

SETUP FOR THE CALCULATIONS

The calculations were performed using the three-dimensional, multi-material Eulerian hydrocode CTH [2]. The setup for the calculations is illustrated in Fig. 1. The target is RHA with dimensions of 330 mm along the shotline direction and 152 mm square in the two lateral directions. The penetrator is WHA with an extended length L_e of 249 mm and collapsed diameter D_c of 7.5 mm. The extension ratio h of the rod, defined as $\eta = (L_e/L_c) - 1$, was set to 0.98 in these simulations, so the corresponding collapsed length L_c of the rod was 126 mm. Thus, the rod shown is one that is assumed to be launched in a collapsed configuration, with length L_c and diameter D_c, then extended sometime during flight to achieve an extended length L_e at impact.
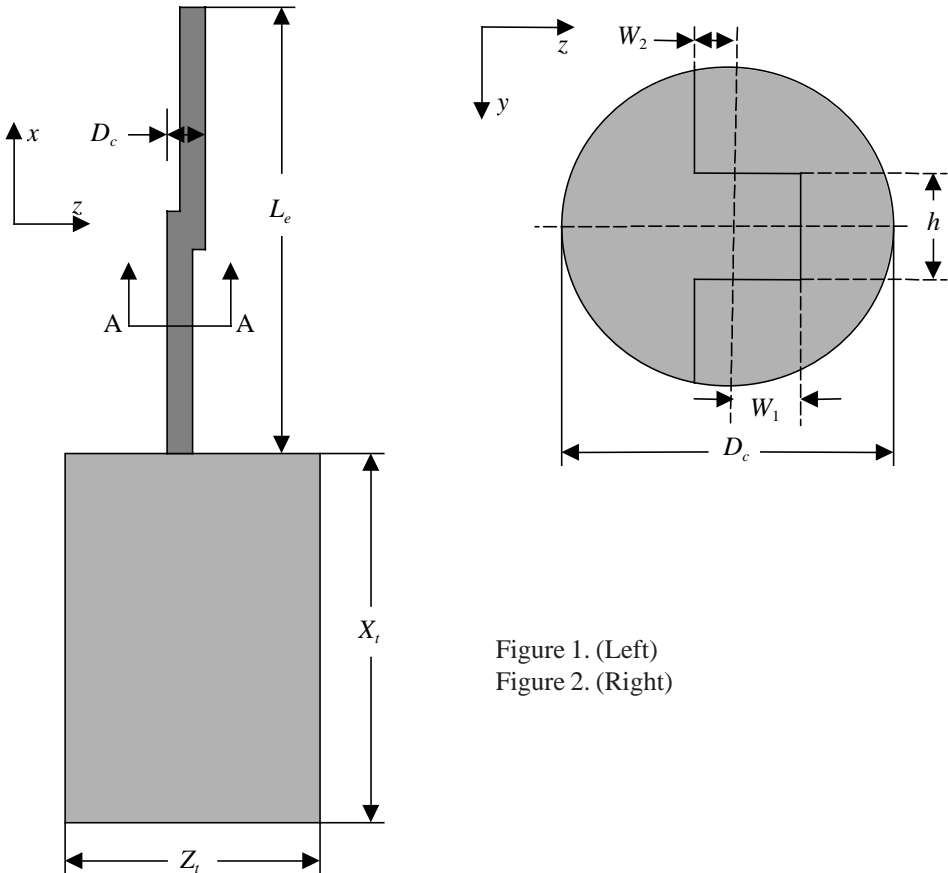
Figure 1. (Left)
Figure 2. (Right)

Details of the cross sections for the fore and aft portions of the penetrator are illustrated in Fig. 2. The cross section consists of a *tongue* on the left side along with a matching *slot* on the right side. For purposes of this paper, the left portion of the penetrator will be referred to as the *T section,* and the right portion the *U section*. The height h of the tongue in the T section was set to $D_c/3$ and was positioned symmetrically with respect to the hori-

zontal axis in these simulations. Also, the cross-sectional areas of the U and T sections were kept equal. As such, the geometry of the U and T sections are fixed with the specification of W_1, the distance from the center plane to the edge of the tongue in the T section. Under these conditions, the dimensions W_1 and W_2 are related by a nonlinear relation of the form

$$\frac{3\pi}{8} - \frac{3}{4}\cos^{-1}\left(\frac{2W_2}{D_c}\right) + \frac{3W_2}{2D_c}\sqrt{1 - \left(\frac{2W_2}{D_c}\right)^2} - \frac{W_2}{D_c} - \frac{W_1}{D_c} = 0. \tag{1}$$

This study considers the effect of parametric variations of W_1 on penetration, with W_1 ranging from 0 to $0.35D_c$; the limit of $W_1 = 0$ corresponding to two equal area hemicylinders, and $W_1 = 0.35D_c$ to aggressive channeling in the U section. A total of six calculations were conducted in this study and are summarized in Table 1. The penetrator mass and extended length were kept fixed in each case. Due to the differences between the U and T cross section geometries for $W_1 \neq 0$, these cases were run both with the T section fore (Calculations 2 and 4) and aft (Calculations 3 and 5). Calculation 6 is the simulation of a constant mass, constant length cylindrical rod that was performed for comparison purposes.

Table 1. Summary of calculations and results.

Calculation #	V (km/s)	L_e (mm)	L_c (mm)	D_c (mm)	W_1/D_c (--)	W_2/D_c (--)	T section location	P (mm)
1	2.2	249	126	7.5	0	0	N/A	277
2	2.2	249	126	7.5	0.18	0.09	fore	292
3	2.2	249	126	7.5	0.18	0.09	aft	246
4	2.2	249	126	7.5	0.35	0.18	fore	267
5	2.2	249	126	7.5	0.35	0.18	aft	231
6	2.2	N/A	249	5.3	N/A	N/A	N/A	289

A few additional features were added to the extending rod simulations (Calculations 1–5). This included cylindrical base and end caps, each with a length and diameter of 3.8 and 9.4 mm, respectively, as well as lands positioned at ten locations along the length of the rod, each with a length and diameter of 1.6 and 9.4 mm, respectively. The purpose of these additions was to replicate the features that might be present on a laboratory device for launching a rod with this configuration.

A 0.98 mm cubical computational mesh was used in the region surrounding the penetrator, as well in regions of strong interaction within the target. Outside the interaction region, the mesh dimensions were permitted to grow at a rate of 5%. This mesh is adequate to provide reasonably resolved computational results for the cylindrical rod [3], and is probably also sufficient for the extending rods, albeit a zoning sensitivity study was not performed. Symmetry of the setup in the *xz* plane was exploited so that only half the problem was run (refer to Figs. 1 and 2 for the orientation of the *xz* plane).

A preliminary investigation showed that the complexity of the penetrator topology made it virtually impossible to sweep it across an Eulerian mesh, particularly at the later

stages of penetration where the aft portion of the rod arrives at the base of the crater. On the other hand, here the target geometry is simple and amenable to advection across the mesh. As such, these simulations were run in "reverse ballistics" mode, wherein the target was given an initial velocity and impacted a stationary penetrator.

RESULTS

Results from the six calculations are summarized in the last column of Table 1, where the penetration depth P is shown for each of the simulations. As is evident from these results, the maximum penetration is achieved for the extending rod with $W_1/D_c = 0.18$ and T section forward, and for the cylindrical rod, where the penetration depths are 292 and 289 mm, respectively. The penetration efficiency based on the extended length is about 1.16, which is consistent with the data found in the archival literature [4]. Penetration depths for the remaining extended rods are degraded from this, the worst case occurring for $W_1/D_c = 0.35$ and T section aft, where the penetration is about 20% lower than its maximum value.

The penetration behavior exhibited by this class of extending configurations is made clearer through and examination of the material plots, shown in Figs. 3 – 5. Figs. 3a – 3c show a time history of the materials at 80, 160 and 300 μs, respectively for Calculation 1, where $W_1 = 0$. As can be seen from this sequence, there is some lateral engagement between the aft section of the penetrator and the sidewall of the cavity produced from the forward section. This imparts lateral momentum to the rod, which skews the base of the crater towards the opposite edge of the channel when the aft portion of the rod begins to penetrate, as can be seen in Figs. 3b – 3c. As such, the deepest point of penetration is no longer coincident with the original shotline. This behavior is characteristic of all the extending geometries considered in this study.
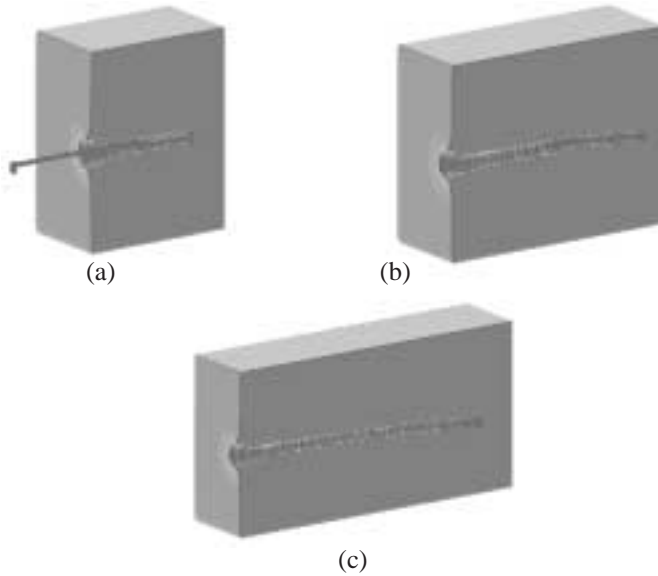
(a)   (b)

(c)

Figure 3. Material plots for $W_1 = 0$ when (a) t = 80 μs, (b) t = 160 μs, and (c) t = 300 μs.

In Figs. 4a – 4c, the material plots are shown at 80, 160 and 300 ms, respectively for Calculation 3, where $W_1 = 0.18D_c$ and the T section is aft. Fig. 4a shows that by 80 μs, the trailing T section of the rod enters the penetration channel, albeit there is less sidewall interaction because the crater dimensions are larger in this plane than those produced for $W_1 = 0$. The lateral momentum imparted to the rod subsequently produces interaction with the opposite edge of the crater, as is seen in Fig. 4b. The interaction is more significant than is seen in Fig. 3b for $W_1 = 0$ since in this case there is a tongue along the bottom edge of the T section that strikes the sidewall first. This re-engagement of the sidewall begins to turn the base of the crater back towards the original shotline, as is seen in Fig. 4c. Clearly, the severity of these lateral interactions would probably fracture the rod at this stage, which is not modeled correctly in this Eulerian code, so the final penetration depth in this case may be somewhat overestimated.
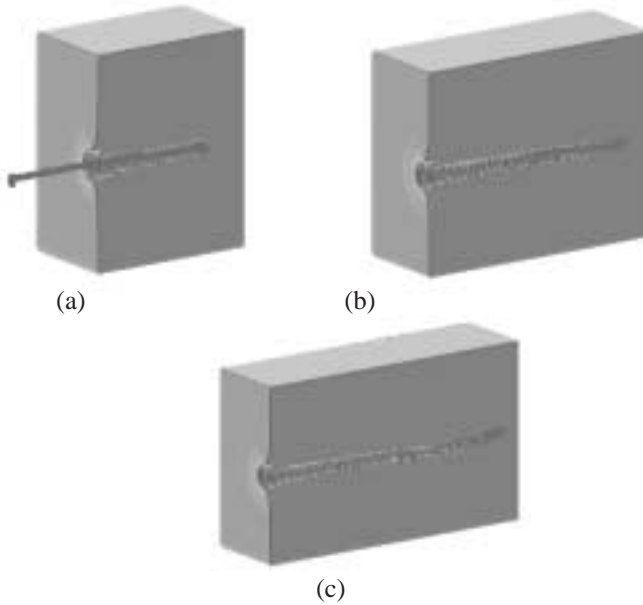
Figure 4. Material plots for $W_1 = 0.18D_c$ and T section aft when (a) t = 80 μs, (b) t = 160 μs, and (c) t = 300 μs.

Much cleaner penetration behavior with very little sidewall interaction is seen when the T section is forward. In Figs. 5a – 5c, the material plots are shown at 80, 160 and 300 μs, respectively for Calculation 2, where $W_1 = 0.18D_c$ and the T section is forward. Fig. 5a shows that by 80 μs, the trailing U section of the rod enters the penetration channel. There is no interaction with the sidewall, but the clearances between the rod and the penetrator are slight. Fig. 5b shows that by 160 μs, the trailing U section begins to penetrate at the base of the crater and, unlike the other two cases, does not engage the opposite edge of the sidewall near the base of the crater. As a result, the base of the final crater, seen in Fig. 5c, is nearly coincident with the original shotline of the rod.

A closer examination of the penetration channel cross-section geometry reveals certain distinguishing characteristics that result in the performance differences seen in Figs. 3–5. Shown in Fig 6a–f are cross sections at 50 and 80 μs of the y-z plane located 25 mm below the original shotline, for the simulations with $W_1 = 0$, $W_1 = 0.18D_c$ with T section aft, and $W_1 = 0.18D_c$ with T section forward (refer to Fig. 1 for the location of the y-z plane). As is evident from Figs. 6a–c, the penetration channel produced by the T section results in a geometry that is nearly cylindrically symmetric and leaves very little residual tungsten along the crater sidewalls to interfere with the trailing section of the rod. The effect of this is seen clearly in Figs. 6d–f, where erosion occurs for the trailing sections in Figs. 6d and 6e.
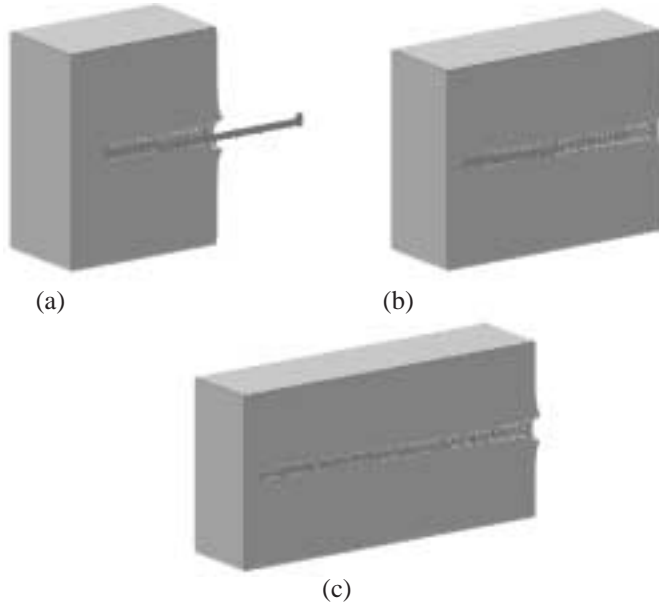
(a)   (b)

(c)

Figure 5. Material plots for $W_1 = 0.18D_c$ and T section forward when (a) t = 80 µs, (b) t = 160 µs, and (c) t = 300 µs.

CONCLUSIONS

The effect of cross section geometry on the penetration of extending hemicylindrical rods has been investigated in this numerical study. The results show that the tongue/slot geometry as well as the orientation can influence the penetration of the rod. The best performance is seen for T sections impacting first, with tongue/slot geometries having intermediate dimensions. The cause for this behavior is made clear through an examination of the rod/target interaction.
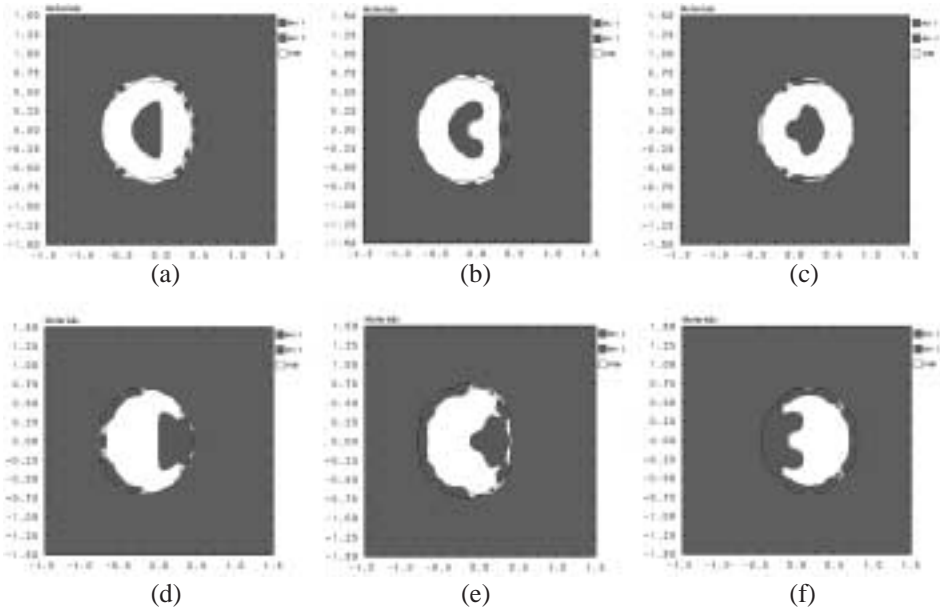
Figure 6. Penetration channel geometry 25 mm below the original target surface for (a) $W_1 = 0$ at 50 μs, (b) $W_1 = 0.18D_c$ with T section aft at 50 μs, (c) $W_1 = 0.18D_c$ with T section forward at 50 μs, (d) $W_1 = 0$ at 80 μs, (e) $W_1 = 0.18D_c$ with T section aft at 80 μs, and (f) $W_1 = 0.18D_c$ with T section forward at 80 μs.

Acknowledgments

REFERENCES

1. D. Barnette, Private communication, 1999
2. J. M. McGlaun, S. L. Thompson, and M. G. Elrick, "CTH: A Three Dimensional Shock Wave Physics Code", *Int. J. Impact Engng 10,* 351–360, 1990
3. D. L. Littlefield and C. E. Anderson, Jr., "A Study of Zoning Requirements for 2-D and 3-D Long-Rod Penetration", *Proceedings of the 1995 APS Topical Conference on Shock Compression of Condensed Matter,* Seattle, WA, August 13–18, 1995
4. C. E. Anderson, B. L. Morris, and D. L. Littlefield, "A Penetration Mechanics Database", *SwRI Report No. 3593/001,* January, 1992